High-efficient flexible pressure sensor based on nanofibers and carbon nanotubes for artificial electronic skin and human motion monitoring

Tao Zhang[1] · Wentao Zhang[1] · Yang Li[1] · Xiulei Hu[1] · Haoxiang Yuan[1] · Tianyan Jiang[1]

Abstract

Flexible pressure sensor plays a crucial role in wearable devices since it converts the physical signals of human motions into electrical signals. Among various pressure sensors, foam-based pressure sensors received great attention due to their excellent flexibility, low weight, and pressure resistance. However, the sensitivity of the foam-based pressure sensor is still not large enough, and the sensing range is also urged to be further improved. Herein, we proposed a high-performance foam-based pressure sensor composed of polydimethylsiloxane (PDMS), multi-walled carbon nanotubes (MWCNT), and nanofibers (FIBER). The PDMS/FIBER@MWCNT foam-based pressure sensor possessed outstanding sensitivity up to 4.07 kPa^{-1} and a wide sensing range of 0–70 kPa. The pressure sensor also presented excellent linearity during 0–20 kPa and 20–70 kPa, respectively. And 2000 cyclic compression tests shown good cyclic stability. Meanwhile, the pressure sensor worked efficiently in monitoring subtle and large human motions, such as finger bending, wrist bending, throat vocal signals, and various pressures. In addition, the pressure sensor owned significant discrimination and high efficiency against different pressure, which is beneficial in human complex motion monitoring and signal analysis of wearable devices. Consequently, the PDMS/FIBER@MWCNT foam-based pressure sensor may possess promising prospects and potential in the applications of artificial electrical skin and wearable devices.

Keywords Flexible pressure sensor · Polydimethylsiloxane foam · Artificial electrical skin · Human motion monitoring · High-efficient wearable device

1 Introduction

In recent years, benefiting from the huge demand for wearable devices, electronic skin, and other human motion monitoring equipment, flexible pressure sensors have received great attention, and development as cutting-edge devices [1–10]. Traditional flexible pressure sensors can be divided into piezoelectric [11, 12], capacitive [13, 14], and piezoresistive [15, 16]. The piezoresistive pressure sensor is deeply studied and applied due to its easy acquisition and analysis of resistance signals, simple manufacturing process, low cost, and high sensitivity [17, 18]. Nowadays, piezoresistive pressure sensors based on various flexible materials are replacing traditional pressure sensors made of metals or semiconductors that cannot be bent over a wide range and are not suitable for monitoring human movements [19–21]. The flexible materials mainly include thermoplastic polyurethane (TPU) and polydimethylsiloxane (PDMS), which have the characteristics of strong flexibility, high reliability, low cost, and harmless to human [22, 23]. Therefore, such flexible materials are very suitable for human motion monitoring and the fabrication of artificial electronic skin. For example, Wang et al. fabricated a pressure sensor based on gold nanoparticle/PDMS by assembling it with graphene Microchannel [24]. The obtained sensor exhibited a wide detection range up to 50 kPa. Although a large number of film pressure sensors have made great progress in sensitivity, they only have high sensitivity to tensile strain, which limits their application fields [25, 26].

Various sensing structures were designed, such as porous structure, wave structure, and filamentary structure, for improving the performance of pressure sensor [27–29]. Among them, the three-dimensional porous structure is widely used due to its excellent pressure resistance and

✉ Tianyan Jiang
jiangtianyan@cqut.edu.cn

1 School of Electrical and Electronic Engineering, Chongqing University of Technology, Chongqing 400054, China

flexibility. In addition, the characteristics of low weight, high stretch, and high resilience are also obtained attributed to the porous structure [30, 31]. Yu et al. fabricated a pressure sensor by combining the fractal electrode with graphene foam [32]. The obtained sensor has high sensitivity and a wide linear range. Chen et al. reported a pressure sensor based on thermoplastic polyurethane (TPU)/ polydopamine (PDA)/MXene conductive composite foam by a combination of directional freezing and dip-coating method [33]. The sensor exhibits excellent flexibility, fast response times (~40 ms), and good durability over 5000 cycles. Furthermore, the composite foam has excellent recognition ability for different compressive strain amplitudes. Recently, great efforts have been made to promote the sensitivity and sensing range of foam-based pressure sensors. For instance, fiber fabrics are employed as substrates to improve the sensitivity in the low-pressure area. Jiang et al. developed a flexible pressure sensor based on hierarchical three-dimensional and porous reduced graphene oxide fiber fabrics [34]. The sensor displayed excellent durability in a wide range of frequencies, a low detection limit (1.17 Pa), and an ultrafast response time (30 ms). In addition, the fiber-to-fiber interfaces can produce a highly sensitive contact resistance, leading to a higher sensitivity at low applied strains. On the other hand, multi-walled carbon nanotubes (MWCNT) are usually adopted as excellent conductive fillers due to their outstanding electrical conductivity and rich three-dimensional structure.

Tian et al. prepared a piezoresistive sensor based on a nonwoven substrate composed of highly crimped bicomponent fibers which adhered multi-walled carbon nanotubes [35]. The sensor exhibits good flexibility, broad dynamic sensing range (0-131.32 kPa), and fast response/relaxation (105/156 ms). Although the sensitivity and sensing range of the pressure sensor have been improved under various strategies, the foam-based pressure sensor with high sensitivity, linearity and wide sensing range still needs further study.

Herein, we fabricated a foam-based piezoresistive pressure sensor based on polydimethylsiloxane (PDMS), nanofibers (FIBER), and multi-walled carbon nanotubes (MWCNT) by salt-templating and dip soaking methods. The obtained PDMS/FIBER@MWCNT foam-based pressure sensor owned a wide sensing range up to 70 kPa, high sensitivity with a value 4.07 kPa^{-1}, and remarkable stability. The pressure sensor also possessed excellent linearity in 0–20 kPa and 20–70 kPa, respectively. Furthermore, the experiments of various words and different speeds of the same action demonstrated that the pressure sensor had significant discrimination and high efficiency against different pressure and vocal signals even the same action at different speeds. Therefore, the PDMS/FIBER@MWCNT foam-based piezoresistive pressure sensor exhibited great

potential in wearable devices, human motion monitoring, and artificial electronic skin.

2 Experimental settings

2.1 Materials and chemicals

Polydimethylsiloxane (PDMS, 99%) (SYLGARDTM 184 Silicone Elastomer Base and curing agents) were purchased from Dow Corning (American). Nanocellulose fiber (FIBER, 2.12%) was purchased from Zhejiang Jinjiahao Green Nanocellulose Co., Ltd. (Zhejiang, China). Multi-walled carbon nanotubes (MWCNT, 14%) were obtained from Nanjing XFNANO Materials Tech CO., Ltd. (Nanjing, China). Potassium Chloride was purchased from Kelong Chemical Co., Ltd. (Chengdu, China). Tris-Base (Tris, 98%) and Sodium lauryl sulfonate (SDS, 99%) were obtained from Fuzhou Phygene Biological Technology Co., Ltd. (Fuzhou, China). Dopamine hydrochloride (DA, 98%) was purchased from Shanghai Aladdin Biochemical Technology Co., Ltd. (Shanghai, China). All the materials and chemicals were used as received.

2.2 Preparation of PDMS/FIBER@MWCNT foam

The preparation of PDMS/FIBER@MWCNT was shown in Fig. 1 (a). Firstly, 3.0 g PDMS prepolymer was mixed with the curing agent at a ratio of 10:1 for 15 min. Besides, 0.5 g purified nanocellulose fiber (31.8 mg/ml) were added to the PDMS solution and stirred for 10 min with magnetic stirrers until fibers and solution are fully mixed and evenly distributed. Secondly, 27 g of potassium chloride were added to the PDMS/FIBER solution and stirred for 10 min to make the solution adhere to the surface of potassium chloride particles uniformly. Then, the mixture was added to the template and treated by vacuum drying oven at 120 °C for 3 h to promote the sample curing. In order to form an abundant pore structure, the salt template method was employed. Third, the cured sample was immersed in deionized water at 80 °C for 12 h until potassium chloride was completely precipitated from the sample. The PDMS/FIBER foams were obtained. Furthermore, the PDMS/FIBER foams were first washed with acetone to remove the impurities of the surface and immersed in DA/TRIS mixed solution (pH≈8.8) at 35 °C for 12 h for the purpose of improving the hydrophilicity of PDMS/FIBER foams and facilitate the adhesion of MWCNT. As a consequence, the polydopamine (PDA) modified PDMS/FIBER foams were obtained. The color of PDMS/FIBER foams turned from white to brown after the deposition of PDA. Moreover, to improve the dispersion of MWCNT, sodium lauryl sulfonate (SDS) and MWCNT

were mixed at a ratio of 1.5:1 under ultrasonication for 30 min. Finally, the PDA-modified PDMS/FIBER foams were immersed into the SDS/MWCNT solution (0.5 mg/ml) under ultrasonication for 10 min repeatedly. Then, the foams were transferred to a drying oven at 70 °C for 1 h, achieving a black porous and conductive PDMS/FIBER@MWCNT foam. Additionally, the different soaking numbers were employed to investigate the effect on the electronic properties of PDMS/FIBER@MWCNT foam.

### 2.3 Fabrication of piezoresistive pressure sensor

The fabrication process of the piezoresistive pressure sensor based on PDMS/FIBER@MWCNT foam was shown in Fig. 1 (b). First, The PDMS prepolymer was mixed with the curing agent at a ratio of 10:1 for 15 min and solidified by vacuum drying oven at 120 °C for 3 h. Second, the conductive copper tape adhered to the surface of PDMS as

an extraction electrode for the pressure sensor. Third, the conductive silver paste was employed as the conjunction of electrode and PDMS/FIBER@MWCNT foam, forming a close junction structure. The silver paste was uniformly distributed on the surface of the copper electrode with the help of a hard template and cured with the PDMS/FIBER@MWCNT foam at 60 °C for 20 min. The electrode on the other side was assembled in the same way. Finally, the piezoresistive pressure sensor based on PDMS/FIBER@MWCNT foam was fabricated.

2.4 Characterizations and measurements

The microstructure and morphology of PDMS/FIBER and PDMS/FIBER@MWCNT foam were characterized by scanning electron microscopy (SEM) (Gemini SEM500, ZEISS, Germany) respectively. The Fourier transform infrared (FTIR) (TENSOR II, BRUKER, USA) was introduced

Fig. 1 (**a**) Schematic diagram for the fabrication process of PDMS/FIBER@MWCNT foam. (**b**) The preparation process of PDMS/FIBER@MWCNT foam-based piezoresistive pressure sensor
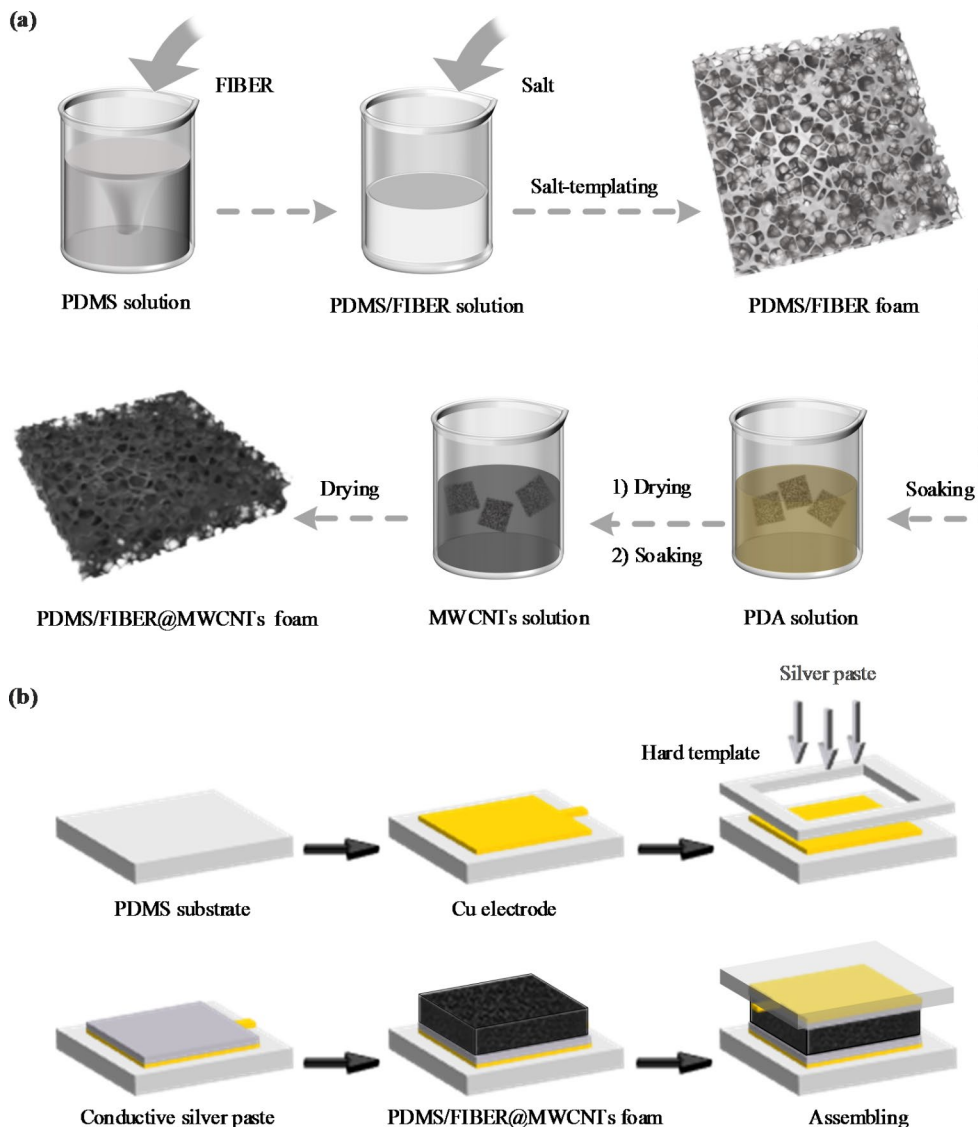
to detail the elemental composition of the foams. The FTIR spectra were obtained in the range of 500–4000 cm^{-1}. The Raman spectrums of the pressure sensor at different manufacturing stages were characterized by Raman spectrometer (LabRAM HR Evolution, HORIBA, France) with laser excitation 530 nm.

The mechanical performance and electric properties of PDMS/FIBER@MWCNT foam were characterized by the universal testing machine (ETM-530B, WANCE, China) and digital source meter (2450, Keithley, USA) respectively. The dynamic change of resistance was recorded by the digital source meter when the testing machine pressed the piezoresistive pressure sensor.

3 Results and discussion

3.1 Structure, morphology and characterizations of PDMS/FIBER@MWCNT foam

As shown in Fig. 2 (a)-(d), the fabrication process of piezoresistive pressure sensor based on PDMS/FIBER@ MWCNT foam consists of four parts, including PDMS/ FIBER foam (a), the PDA modified PDMS/FIBER foam

(b), PDMS/FIBER@MWCNT foam (c) and the piezoresistive pressure sensor encapsulated by PDMS (d). Figure 2 (a) shows the macrostructure of PDMS/FIBER foam, the obviously abundant pore structure was formed by the salt-templating method. The SEM images of PDMS/FIBER foam were displayed in Fig. 2 (e)-(g), indicating the porous structure and nanofibers were evenly arranged inside the foam. Figure 2 (b) shows the PDA-modified PDMS/FIBER foam, the color turned brown due to the deposition of PDA. The PDA was introduced to promote the hydrophilicity of PDMS/FIBER foam and facilitate the adhesion between MWCNT and PDMS/FIBER foam [36]. Compared with the smooth surface shown in Fig. 2 (g), Fig. 2 (i) and (j) indicated the self-polymerization of PDA on the surface of PDMS/FIBER foam. And the porous structure was no apparent changes. The employment of MWCNT led the PDA-modified PDMS/FIBER foam turned to black, which indicated the MWCNT adhered to the surface of PDMS/ FIBER foam successfully as shown in Fig. 2 (c). According to Fig. 2 (h) and (k), the PDMS/FIBER@MWCNT foam inherited the porous structure after the ultrasonic immersion of MWCNT solution, but the edge structure is sharper than before. Meanwhile, Fig. 2 (l) and (m) exhibited the abundant MWCNT and also demonstrated that PDMS/FIBER

Fig. 2 Characterizations of sensor materials. (**a**)-(**c**) The surface morphology of PDMS/ FIBER foam, PDA-modified PDMS/FIBER foam, and PDMS/ FIBER@MWCNT foam, respectively. (**d**) Schematic diagram of the pressure sensor. (**e**)-(**g**) SEM images of PDMS/FIBER foam. (**h**)-(**j**) SEM images of PDA modified PDMS/FIBER foam. (k)-(m) SEM images of PDMS/ FIBER@MWCNT foam
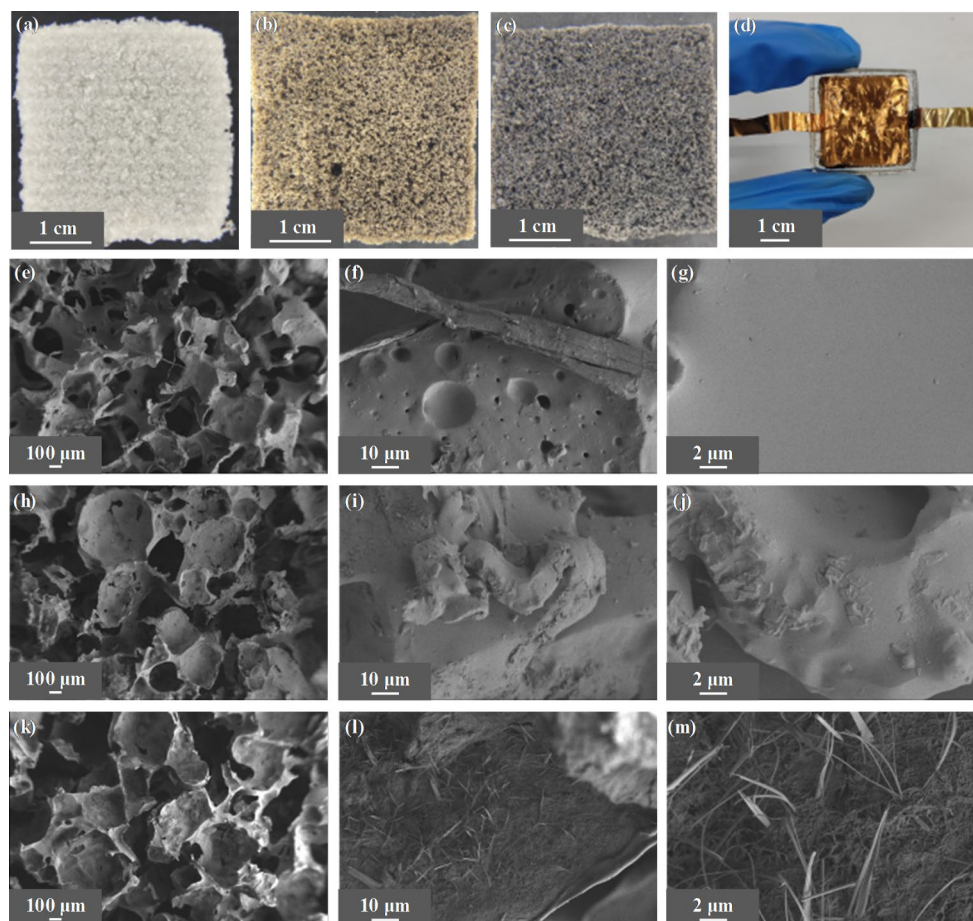
foam was adsorbed by MWCNT tightly, which brought the PDMS/FIBER@MWCNT foam pressure sensing capacity.

3.2 Sensing mechanism of PDMS/FIBER@MWCNT foam-based pressure sensor

Figure 3 (a) presented the Fourier-transform infrared (FTIR) spectrum of the PDMS/FIBER@MWCNTs foam, the characters adsorption peaks of PDMS were clearly recognized. The stretching band of -CH$_3$ (1385 cm^{-1}), Si-O-Si (1097 cm^{-1}) were all apparently observed. Meanwhile, the characters adsorption peaks of FIBER which also revealed in Fig. 3 (a). the -CH$_2$- (2962 cm^{-1}) and -C-O- (1060 cm^{-1}) were also easily identified. However, the peaks of MWCNTs were hardly observed in the FTIR spectrum, which may be attributed to low content of MWCNTs and the weak sensitivity of FTIR to it. Whereas, the adsorption peaks of -CH$_3$ and -CH$_2$- were shift to 1372 cm^{-1} and 2948 cm^{-1} in the PDMS/FIBER@MWCNTs foam, respectively. Indicating the strong hydrogen bonds were generated between MWCNTs and PDMS/FIBER foam. The Raman spectrum of PDMS/FIBER@MWCNTs foam was presented in Fig. 3 (b). The D-band (1375.5 cm^{-1}) and G-band (1580.7 cm^{-1}) of MWCNTs were obviously observed, and the peaks also appeared in the PDMS/FIBER@MWCNTs foam, which demonstrated the MWCNTs were successfully included in the composite foam.

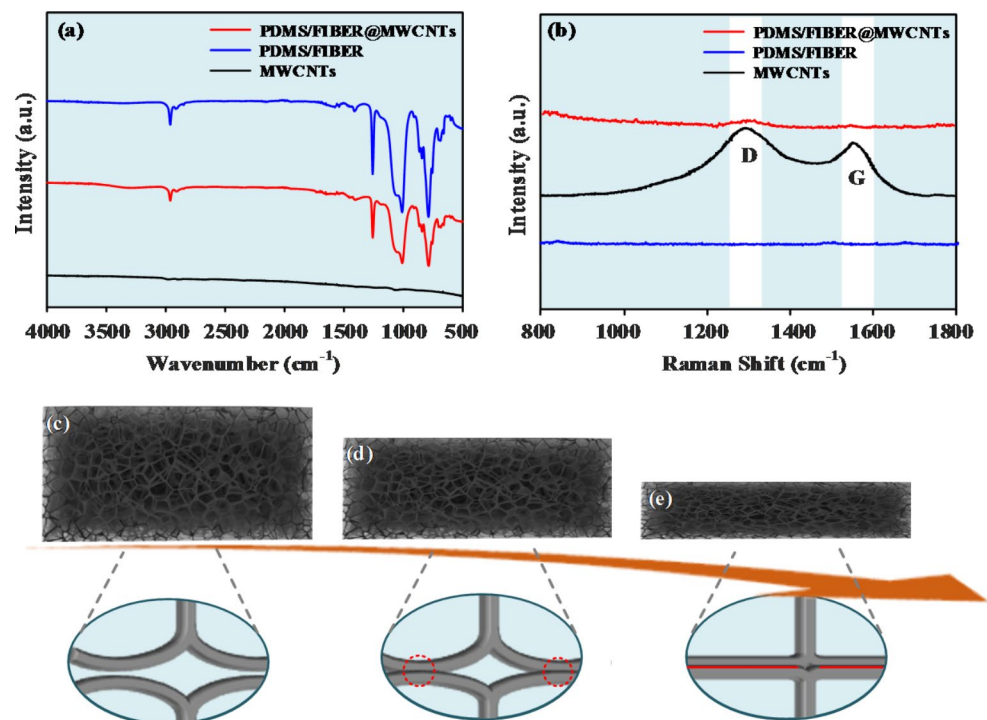Figure 3 (c)-(e) presented the pressure sensor base on PDMS/FIBER@MWCNT foam in the initial state, low-stress state, and high-stress state, respectively. In the initial state, the pressure sensor formed conductive pathways through the foam skeleton which was attached by the MWCNT. The foam skeleton was connected to the electrode by conductive silver paste on the foam surface, realizing the transmission of resistance signal. In the low-stress state, the pore structure was compressed due to the external pressure, and new conductive points formed by the contact of the inner wall of the pore structure. As shown in Fig. 3 (d), the new conductive pathways were formed, decreasing the resistance of PDMS/FIBER@MWCNT foam. Under high pressure, the pore structure was further compressed with the increase of pressure, the conductive areas were further expanded. Resulting in the generations of more conductive pathways and leading to the further decrease of resistance. Eventually, the resistance approached a minimum value and no longer decreased with the increase of pressure.

3.3 Piezoresistive performance of PDMS/FIBER@MWCNT foam-based pressure sensor

The mechanical and electrical joint testing platform was established to explore the sensing performance of PDMS/FIBER@MWCNT foam. And the measurement results, including sensitivity, stability, and other properties were presented in Fig. 4. Meanwhile, the sensitivity (S) of the pressure sensor can be defined as the Eq. (1):

$$S = \frac{\delta\left[\Delta R/R_0\right]}{\delta P} = \frac{\delta\left[\left(R_0 - R\right)/R_0\right]}{\delta P} \tag{1}$$

Fig. 3 (**a**) FTIR spectrum, and (**b**) Raman spectrum of PDMS/FIBER@MWCNT foam. (**c**) Schematic evolutions of the PDMS/FIBER@MWCNT foam with the increase of pressure

Where R_0 was the initial resistance of the pressure sensor when the force was not applied on. R symbolized the current resistance when the pressure was applied to the sensor. P represented the current pressure which applied to the sensor. Meanwhile, to reflect the sensitivity of the pressure sensor in different pressure ranges more accurately, the sensitivity in the range of 0–20 kPa was defined as S_1, and the sensitivity in the range of 20–70 kPa was defined as S_2.

Different soaking times (2, 4, 6) were designed to investigate the effects of adsorption quantities of MWCNT on the sensor's sensitivity. Figure 4 (a) revealed the sensitivity of the pressure sensor with different soaking times. The pressure sensor after 4 times soaking had the highest sensitivity in the pressure range of 0–20 kPa with a value of 4.07 kPa^{-1}, and 0.69 kPa^{-1} in the range of 20–70 kPa. The sensitivity of soaked 2 times and 6 times were 1.58 kPa^{-1} and 1.50 kPa^{-1} in the pressure range of 0–20 kPa, respectively. It is obvious that the sensitivity of the pressure sensor increased as the increase of soaking times. However, the sensitivity displayed a decrease when the foams beyond 4 times soaking. In summary, when a small amount of MWCNTs adhere to the inner wall of the foam, a small quantity of MWCNTs can only form fewer conductive paths, resulting in insufficient sensitivity. However, with the increase of the content of MWCNTs, a rich three-dimensional structure is formed inside the foam, and a stable conductive path can be formed in time under external pressure, resulting in higher sensitivity. Whereas, with the further increase of the content of MWCNTs, the conductivity of the pressure sensor is greatly enhanced after the foam is filled with MWCNTs, which means that it is difficult to form a new conductive path under external pressure, resulting in a decrease in sensitivity. Meanwhile, the sensitivity was gradually declined with the pressure increase when the pressure higher than 20 kPa. Nevertheless, the linearity of the pressure sensor was much better in a wide pressure range of 20–70 kPa. As a consequence, the pressure sensor based on PDMS/FIBER@MWCNT foam owned a considerable sensitivity with a value 4.07 kPa^{-1} in the range of 0–20 kPa, and reliable linearity at the range of 20–70 kPa. Thus, the 4 times soaking pressure sensor was designed as the appropriate sample, conducting the following tests.

Figure 4 (b) revealed the response and recovery time of the pressure sensor with 3.5 kPa. The pressure sensor based on PDMS/FIBER@MWCNT foam possessed a response time and recovery time of 41 ms and 60 ms, respectively. The dynamic response performance was an important aspect of the application for the pressure sensor. Figure 4 (c) presented the dynamic response performance of the sensor under 5 kPa, 10 kPa, and 30 kPa, respectively. The rapid response performance at 350 mm/s and 500 mm/s under 8 kPa were shown in Fig. 4 (d) and (e). It could be seen that

the pressure sensor has considerable repeatability and a significantly different response to different pressure. According to Fig. 4 (f), the dynamic cycling performance of the pressure sensor was tested at a pressure range of 0–30 kPa for 2000 cycles. The signals for the time range of 2990–3010 s were placed in Fig. 4 (g), and no obvious distortion throughout the cycle. The response of the pressure sensor could keep stable, which demonstrated that the pressure sensor based on PDMS/FIBER@MWCNT foam maintained excellent stability and qualified for long-term work. Meanwhile, the sensitivity of PDMS/FIBER@MWCNT foam-based pressure sensor in this work was better than the relevant pressure sensors researched previously according to Table 1.

3.4 Applications of PDMS/FIBER@MWCNT foam-based pressure sensor

To demonstrate the pressure sensor based on PDMS/FIBER@MWCNT foam has the capacity of monitoring human body motions. The pressure sensor was adhered to fingers, wrists, and throat to capture their movements. Meanwhile, to test the pressure sensor's response to different actual pressures, different weights were employed. As shown in Fig. 5 (a), the weight of 50 g, 100 g, and 200 g was applied to the pressure sensor respectively. It could be seen that the pressure sensor had a significantly different response to various pressure changes. Meanwhile, the resistance curves could keep stable in a certain range, which proved that the pressure sensor could identify different weights. Figure 5 (b) presented the response curve when the pressure sensor was assigned to monitor the body action of finger bending and wrist bending. The sensor displayed different response curves for distinct actions, which also indicated that the pressure sensor could distinguish different human movements. Furthermore, according to Fig. 5 (c), the pressure sensor detected the different vocal signals of the throat successfully.

Testing sentences "How are you", "Welcome" and "Fine, thanks" were included and conducted in the experiment. The vocal features of different sentences were effectively captured according to the response curves, demonstrating the pressure sensor could also detect weak vocal signals of human body.

The piezoresistive pressure sensor based on PDMS/FIBER@MWCNT foam was proved to have the potential of monitoring the body movements of human according to experimental results. Thus, the artificial electronic skin was designed to simulate the human skin which could distinguish various pressure. As shown in Fig. 5 (d), the pressure sensor was arranged in matrix form of 5×5 to investigate its potential applications for artificial electronic skin. The artificial electronic skin schematic was exhibited in Fig. 5 (g).

Fig. 4 (**a**) Sensitivity of pressure sensor. (**b**) Dynamic response and recovery time under 3.5 kPa. (**c**) Dynamic response performance under 5 kPa, 10 kPa, and 30 kPa, respectively. (**d**)-(**e**) Dynamic response curves at 350 mm/s and 500 mm/s, respectively. (**f**) Dynamic cycling performance between 0–30 kPa. (**g**) Magnified view for the time range of 2990–3010 s
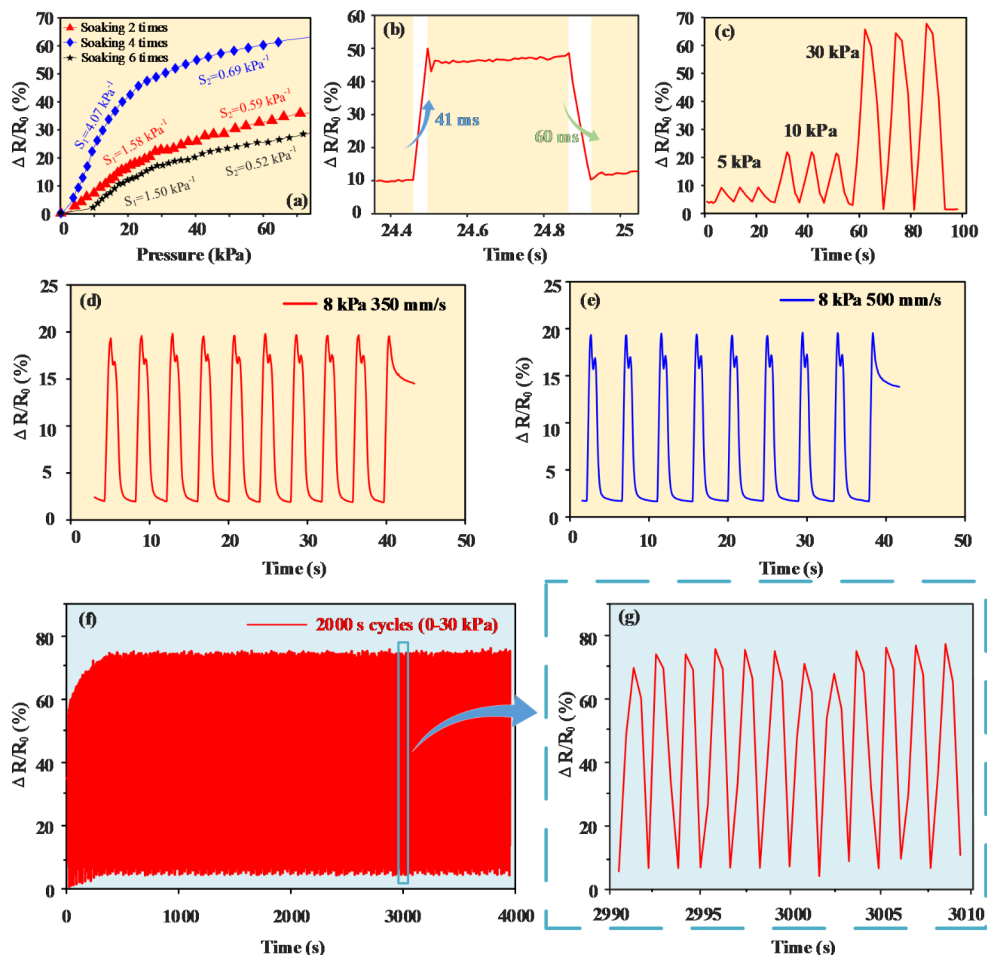

Table 1 Comparison with the sensitivity of relevant pressure sensors in recent studies

Sensitive materials	Sensitivity	Pressure range	Response/ recovery time	Year	Reference
PDMS/FIBER@MWCNT	4.07 kPa^{-1}	0–20 kPa	40 ms	2022	This work
	0.69 kPa^{-1}	20–70 kPa	61 ms		
MXene@PDMS	2.6 kPa^{-1}	0–30 kPa	40 ms	2022	[37]
PS-rGO	1.41 kPa^{-1}	0–50 kPa	20 ms	2022	[38]
Ti$_3$C$_2$Tx/MWCNT	0.2 kPa^{-1}	0.035–316.7 kPa	200 ms	2022	[39]
			900 ms		
CNT-embedded TPU	1.02 kPa^{-1}	0.7 Pa–160 kPa	65 ms	2021	[40]
			29 ms		
PB	0.614 kPa^{-1}	0–6 kPa	235 ms	2021	[41]
	0.064 kPa^{-1}	6–40 kPa	250 ms		
CNT film	2.51 kPa^{-1}	0–10 kPa	84 ms	2021	[42]
			117 ms		
CNF/PDMS	0.6 kPa^{-1}	0–1 kPa	30 ms	2021	[43]
	0.08 kPa^{-1}	1–6 kPa	25 ms		
FW/rGO	1.85 kPa^{-1}	0–60 kPa	150 ms	2020	[44]
rGO-CB@LS	0.66 kPa^{-1}	0-0.5 kPa	420 ms	2020	[45]
	1.89 kPa^{-1}	0.5–2 kPa	290 ms		

According to Fig. 5 (e), double 200 g and double 20 g and other weights were placed onto the surface of artificial electronic skin. It could be clearly found that the different magnitudes and different positions of the external pressure are accurately monitored. Meanwhile, the relative variation of resistance was in agreement with the actual weight and position as shown in Fig. 5 (h). Similarly, the weight of 500 g was fixed on the surface of the electronic skin and could

Fig. 5 Applications of the wearable device based on the pressure sensor. (**a**) Applications of the pressure sensor in the detection of different weights. (**b**) Wearable applications of the pressure sensor in monitoring human motions. (**c**) Wearable applications of the pressure sensor in the identification of throat vocalization. (**d**)-(**i**) Applications of the pressure sensor in artificial electrical skin
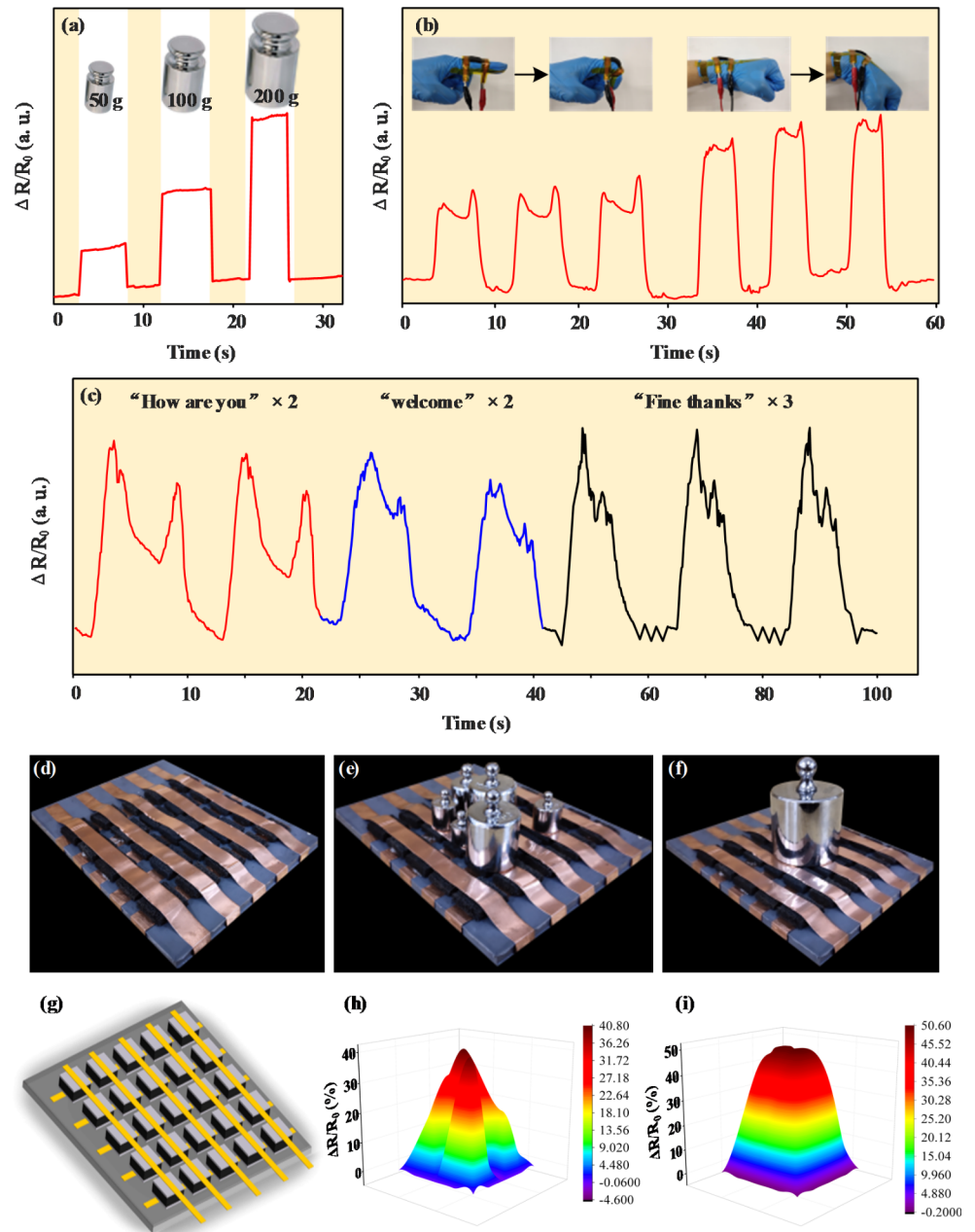
be found to be precisely monitored according to Fig. 5 (i). The results demonstrated that the artificial electronic skin based on PDMS/FIBER@MWCNT foam has great potential in monitoring the pressure and position of the external object. Consequently, the pressure sensor based on PDMS/FIBER@MWCNT foam owned the capacity of monitoring human body movements, even the weak vocal signals from the throat. And the piezoresistive pressure sensor also has a promising prospect in the artificial electronic skin field.

4 Conclusion

In summary, the PDMS/FIBER@MWCNT foam was fabricated by dipping the PDMS/FIBER foam into MWCNT solution and successfully applied as a pressure sensor to monitor the pressure changes and human movements with high sensitivity. The electrical and mechanical properties of the conductive PDMS/FIBER@MWCNT foam could be improved by adjusting the number of soaks. The sensing performance was improved by increasing the soaking number and reached the optimum after 4 times soaking. The pressure sensor possessed a high sensitivity up to $4.07\ kPa^{-1}$ and a wide sensing range of 0–70 kPa. In addition, the

pressure sensor also displayed excellent linearity and cyclic stability. The applications of the pressure sensor in monitoring human movements, such as finger bending, wrist bending, throat vocal vibration, and different pressures, were also demonstrated. Moreover, the sensor owns remarkable discrimination and high efficiency for different pressure and vocal signals, even the same pressure level at different speeds, which was suitable for human complex motion monitoring. It should be noted that the conductive foam also exhibited great potential in the artificial electronic skin. consequently, it is believed that the pressure sensor has broad application prospects in the field of wearable devices in the future.

Author contributions Tao Zhang: Conceptualization, Methodology, Investigation, Writing e original draft. Wentao Zhang: Investigation. Yang Li: Formal analysis, Visualization. Xiulei Hu: Formal analysis. Haoxiang Yuan: Software. Tianyan Jiang: Validation, Writing-review & editing, Project administration, Funding acquisition.

Declarations

Competing interests The authors declare that they have no known competing financial interests or personal relationships that could have appeared to influence the work reported in this paper.

References

1. Z. Wang, Z. Zhou, S. Wang, X. Yao, X. Han, W. Cao et al., An anti-freezing and strong wood-derived hydrogel for high-performance electronic skin and wearable sensing. Compos. B Eng. **239**, 109954 (2022). https://doi.org/10.1016/j.compositesb.2022.109954

2. D. Nahavandi, R. Alizadehsani, A. Khosravi, U.R. Acharya, Application of artificial intelligence in wearable devices: Opportunities and challenges. Comput. Meth Programs Biomed. **213**, 106541 (2022). https://doi.org/10.1016/j.cmpb.2021.106541

3. G. Wang, L.Q. Tao, Z. Peng, C. Zhu, H. Sun, S. Zou et al., Nomex paper-based double-sided laser-induced graphene for multifunctional human-machine interfaces. Carbon **193**, 68–76 (2022). https://doi.org/10.1016/j.carbon.2022.03.026

4. W. Cao, Z. Wang, X. Liu, Z. Zhou, Y. Zhang, S. He et al., Bioinspired MXene-Based user-interactive electronic skin for Digital and Visual Dual-Channel sensing, Nano-Micro Lett. 14 (119) (2022). https://doi.org/10.1007/s40820-022-00838-0

5. R. Sun, L. Gao, F. Liu, H. Su, L. Wu, Z. Zou et al., Magnetically induced robust anisotropic structure of multi-walled carbon nanotubes/Ni for high-performance flexible strain sensor. Carbon **194**, 185–196 (2022). https://doi.org/10.1016/j.carbon.2022.03.032

6. H. Zhao, G. Zhu, F. Li, Y. Liu, M. Guo, L. Zhou, R. Liu, Sridhar Komarneni, 3D interconnected honeycomb-like ginkgo nut-derived porous carbon decorated with β-cyclodextrin for ultrasensitive detection of methyl parathion. Sens. Actuators B **380**, 133309 (2023). https://doi.org/10.1016/j.snb.2023.133309

7. H. Zhao, M. Guo, F. Li, Yu Zhou, G. Zhu, Y. Liu, Q. Ran, F. Nie, V. Dubovyk, Fabrication of gallic acid electrochemical sensor based on interconnected Super-P carbon black@mesoporous silica nanocomposite modified glassy carbon electrode. J. Mater. Res. Technol. **24**, 2100–2112 (2023). https://doi.org/10.1016/j.jmrt.2023.03.129

8. Q. Yunhang Liu, G. Wang, Q. Zhu, F. Ran, M. Li, G. Guo, H. Wang, Zhao, Novel electrochemical sensing platform based on palygorskite nanorods/Super P Li carbon nanoparticles-graphitized carbon nanotubes nanocomposite for sensitive detection of niclosamide. Ceram. Int (2023). https://doi.org/10.1016/j.ceramint.2023.03.253

9. L. Jingjing Liu, J. Zhang, F.B. Zhu, J. Yu, Triethylamine gas sensor based on Pt-functionalized hierarchical ZnO microspheres. Sens. Actuators B **331**, 129425 (2021). https://doi.org/10.1016/j.snb.2020.129425

10. Z. Duan, H. Jiang, Yadong, Tai, Recent advances in humidity sensors for human body related humidity detection. J. Mater. Chem. C **9**, 14963–14980 (2021). https://doi.org/10.1039/D1TC04180K

11. E.S. Hosseini, L. Manjakkal, D. Shakthivel, R. Dahiya, Glycine – Chitosan-Based flexible biodegradable Piezoelectric pressure Sensor. ACS Appl. Mater. Interfaces **12**, 9008–9016 (2020). https://doi.org/10.1021/acsami.9b21052

12. K. Song, R. Zhao, Z.L. Wang, Y. Yang, Conjuncted pyro-piezoelectric effect for self-powered simultaneous temperature and pressure sensing. Adv. Mater. **31**, 1902831 (2019). https://doi.org/10.1002/adma.201902831

13. S.R.A. Ruth, L. Beker, H. Tran, V.R. Feig, N. Matsuhisa, Z. Bao, Rational design of capacitive pressure sensors based on pyramidal Microstructures for Specialized Monitoring of Biosignals. Adv. Funct. Mater. **30**, 1903100 (2020). https://doi.org/10.1002/adfm.201903100

14. J. Yang, S. Luo, X. Zhou, J. Li, J. Fu, W. Yang et al., Flexible, tunable, and Ultrasensitive Capacitive pressure sensor with Microconformal Graphene Electrodes. ACS Appl. Mater. Interfaces **11**, 14997–15006 (2019). https://doi.org/10.1021/acsami.9b02049

15. M. Cao, J. Su, S. Fan, H. Qiu, D. Su, L. Li, Wearable piezoresistive pressure sensors based on 3D graphene. Chem. Eng. J. **406**, 126777 (2021). https://doi.org/10.1016/j.cej.2020.126777

16. J.S. Kim, Y. So, S. Lee, C. Pang, W. Park, S. Chun, Uniform pressure responses for nanomaterials-based biological on-skin flexible pressure sensor array. Carbon **181**, 169–176 (2021). https://doi.org/10.1016/j.carbon.2021.04.096

17. M. Lu, H. Mei, S. Zhou, T. Zhao, L. Cheng, L. Zhang, Activation of percolation network in structural-strengthened polymer-derived ceramic for minor deformation detection. Carbon **183**, 368–379 (2021). https://doi.org/10.1016/j.carbon.2021.07.023

18. Z. Wang, S. Guo, H. Li, B. Wang, Y. Sun, Z. Xu et al., The Semiconductor/Conductor Interface Piezoresistive Effect in an Organic transistor for highly sensitive pressure sensors. Adv. Mater. **31**, 1805630 (2019). https://doi.org/10.1002/adma.201805630

19. W.A.D.M. Jayathilaka, K. Qi, Y. Qin, A. Chinnappan, W.S. García, C. Baskar et al., Significance of Nanomaterials in Wearables: a review on Wearable Actuators and Sensors. Adv. Mater. **31**, 1805921 (2019). https://doi.org/10.1002/adma.201805921

20. H. Guo, Y.J. Tan, G. Chen, Z. Wang, G.J. Susanto, H.H. See et al., Artificially innervated self-healing foams as synthetic piezo-impedance sensor skins. Nat. Commun. **11**, 5747 (2020). https://doi.org/10.1038/s41467-020-19531-0

21. C.S. Boland, U. Khan, C. Backes, A. O'Neill, J. McCauley, S. Duane et al., Sensitive, High-Strain, high-rate Bodily Motion Sensors based on Graphene–Rubber Composites. ACS Nano **8**(9), 8819–8830 (2014). https://doi.org/10.1021/nn503454h

22. C. Armbruster, M. Schneider, S. Schumann, K. Gamerdinger, M. Cuevas, S. Rausch et al., Characteristics of highly flexible PDMS membranes for long-term mechanostimulation of biological

tissue. J. Biomed. Mater. Res. **91**, 700–705 (2009). https://doi.org/10.1002/jbm.b.31446

23. M.P. Wolf, G.B. Salieb-Beugelaar, P. Hunziker, PDMS with designer functionalities—Properties, modifications strategies, and applications. Prog Polym. Sci. **83**, 97–734 (2018). https://doi.org/10.1016/j.progpolymsci.2018.06.001

24. J. Wang, C. Zhang, D. Chen, M. Sun, N. Liang, Q. Cheng et al., Fabrication of a sensitive strain and pressure sensor from Gold nanoparticle-assembled 3D-Interconnected Graphene Microchannel-Embedded PDMS, ACS appl. Mater. Interfaces **12**(46), 51854–51863 (2020). https://doi.org/10.1021/acsami.0c16152

25. X. Shi, H. Wang, X. Xie, Q. Xue, J. Zhang, S. Kang et al., Bioinspired Ultrasensitive and Stretchable MXene-Based strain Sensor via Nacre-Mimetic Microscale "Brick-and-Mortar" Architecture. ACS Nano **13**(1), 649–659 (2019). https://doi.org/10.1021/acsnano.8b07805

26. E. Roh, B.U. Hwang, D. Kim, B.Y. Kim, N.E. Lee, Stretchable, transparent, ultrasensitive, and patchable strain sensor for human–machine Interfaces comprising a nanohybrid of Carbon Nanotubes and Conductive Elastomers. ACS Nano **9**(6), 6252–6261 (2015). https://doi.org/10.1021/acsnano.5b01613

27. Q.J. Sun, X.H. Zhao, Y. Zhou, C.C. Yeung, W. Wu, S. Venkatesh et al., Fingertip-skin-inspired highly sensitive and multifunctional sensor with hierarchically structured conductive Graphite/Polydimethylsiloxane foams. Adv. Funct. Mater. **29**, 1808829 (2019). https://doi.org/10.1002/adfm.201808829

28. Y. Ding, T. Xu, O. Onyilagha, H. Fong, Z. Zhu, Recent advances in flexible and wearable pressure sensors based on piezoresistive 3D monolithic conductive sponges. ACS Appl. Mater. Interfaces **11**(7), 6685–6704 (2019). https://doi.org/10.1021/acsami.8b20929

29. Y. Han, Y. Han, X. Zhang, L. Li, C. Zhang, J. Liu et al., Fish gelatin based Triboelectric Nanogenerator for Harvesting Biomechanical Energy and Self-Powered sensing of human physiological signals. ACS Appl. Mater. Interfaces **12**(14), 16442–16450 (2020). https://doi.org/10.1021/acsami.0c01061

30. Y. Pang, H. Tian, L. Tao, Y. Li, X. Wang, N. Deng et al., Flexible, highly sensitive, and wearable pressure and strain sensors with Graphene Porous Network structure. ACS Appl. Mater. Interfaces **8**(40), 26458–26462 (2016). https://doi.org/10.1021/acsami.6b08172

31. D. Cho, J. Park, J. Kim, T. Kim, J. Kim, I. Park et al., Three-dimensional continuous conductive nanostructure for highly sensitive and stretchable strain Sensor. ACS Appl. Mater. Interfaces **9**(20), 17369–17378 (2017). https://doi.org/10.1021/acsami.7b03052

32. T. Yu, D. Zhang, Y. Wu, S. Guo, F. Lei, Y. Li et al., Graphene foam pressure sensor based on fractal electrode with high sensitivity and wide linear range. Carbon **182**, 497–505 (2021). https://doi.org/10.1016/j.carbon.2021.06.049

33. Q. Chen, Q. Gao, X. Wang, D.W. Schubert, X. Liu, Flexible, conductive, and anisotropic thermoplastic polyurethane/polydopamine /MXene foam for piezoresistive sensors and motion monitoring, COMPOS PART A-APPL S 155 (2022) 106838. https://doi.org/10.1016/j.compositesa.2022.106838

34. X. Jiang, Z. Ren, Y. Fu, Y. Liu, R. Zou, G. Ji et al., Highly compressible and sensitive pressure sensor under large strain based on 3D porous reduced graphene oxide Fiber fabrics in wide Compression strains. ACS Appl. Mater. Interfaces **11**(40), 37051–37059 (2019). https://doi.org/10.1021/acsami.9b11596

35. G. Tian, L. Zhan, J. Deng, H. Liu, J. Li, J. Ma et al., Coating of multi-wall carbon nanotubes (MWCNT) on three-dimensional,

bicomponent nonwovens as wearable and high-performance piezoresistive sensors. Chem. Eng. J. **425**, 130682 (2021). https://doi.org/10.1016/j.cej.2021.130682

36. L. Li, C. Zhu, Y. Wu, J. Wang, T. Zhang, Y. Liu, A conductive ternary network of a highly stretchable AgNWs/AgNPs conductor based on a polydopamine-modified polyurethane sponge. RSC Adv. **5**(77), 62905–62912 (2015). https://doi.org/10.1039/C5RA10961B

37. B. Chen, L. Zhang, H. Li, X. Lai, X. Zeng, Skin-inspired flexible and high-performance MXene@polydimethylsiloxane piezoresistive pressure sensor for human motion detection. J. Colloid Interface Sci. **617**, 478–488 (2022). https://doi.org/10.1016/j.jcis.2022.03.013

38. Y. Long, S.Y. Xia, Z. Huang, C.H. Li, G. He, X. Ma et al., Pomegranate-inspired biomimetic pressure sensor arrays with a wide range and high Linear Sensitivity for Human–Machine Interaction. IEEE Trans. Electron. Devices **69**(3), 1353–1358 (2022). https://doi.org/10.1109/TED.2022.3146108

39. P. Li, H. Zheng, X. Zhao, R. Ding, F. Xue, J. Xiong et al., Wide range pressure sensor construction based on tension-compression conversion and gradient stiffness design strategy. Compos. Part. A Appl. Sci. Manuf. **161**, 107082 (2022). https://doi.org/10.1016/j.compositesa.2022.107082

40. Y.M. Yin, H.Y. Li, J. Xu, C. Zhang, F. Liang, X. Li et al., Facile fabrication of flexible pressure sensor with programmable lattice structure. ACS Appl. Mater. Interfaces **13**, 10388–10396 (2021). https://doi.org/10.1021/acsami.0c21407

41. Z. Duan, Y. Jiang, Q. Huang, S. Wang, Y. Wang, H. Pan et al., Paper and carbon ink enabled low-cost, eco-friendly, flexible, multifunctional pressure and humidity sensors. Smart Mater. Struct. **30**(5), 055012 (2021). https://doi.org/10.1088/1361-665X/abe87d

42. Z. Zhang, X. Gui, Q. Hu, L. Yang, R. Yang, B. Huang et al., Highly sensitive capacitive pressure Sensor based on a Micropyramid array for Health and Motion Monitoring. Adv. Electron. Mater. **7**, 2100174 (2021). https://doi.org/10.1002/aelm.202100174

43. S.W. Dai, Y.L. Gu, L. Zhao, W. Zhang, C.H. Gao, Y.X. Wu et al., Bamboo-inspired mechanically flexible and electrically conductive polydimethylsiloxane foam materials with designed hierarchical pore structures for ultra-sensitive and reliable piezoresistive pressure sensor. Compos. B Eng. **225**, 109243 (2021). https://doi.org/10.1016/j.compositesb.2021.109243

44. H. Guan, J. Meng, Z. Cheng, X. Wang, Processing Natural Wood into a high-performance flexible pressure Sensor. ACS Appl. Mater. Interfaces **12**(41), 46357–46365 (2020). https://doi.org/10.1021/acsami.0c12561

45. M. Cao, S. Fan, H. Qiu, D. Su, L. Li, J. Su, CB nanoparticles optimized 3D wearable Graphene Multifunctional Piezoresistive Sensor framed by Loofah Sponge. ACS Appl. Mater. Interfaces **12**, 36540–36547 (2020). https://doi.org/10.1021/acsami.0c09813